A sestrin-dependent Erk/Jnk/p38 MAPK activation complex inhibits immunity during ageing

Alessio Lanna[1,2,*], **Daniel C O Gomes**[1,3], **Bojana Muller-Durovic**[1], **Thomas McDonnell**[1], **David Escors**[1,4], **Derek W Gilroy**[5], **Jun Hee Lee**[6], **Michael Karin**[7], and **Arne N Akbar**[1,*]

[1]Division of Infection and Immunity, University College London, London, United Kingdom

[2]Nuffield Department of Medicine, University of Oxford, Oxford. United Kingdom

[3]Núcleo de Doenças Infecciosas/ Núcleo de Biotecnologia, Universidade Federal do Espírito Santo - UFES, Vitória- Brazil

[4]Navarrabiomed-Biomedical Research Centre. Fundación Miguel Servet. IdisNA. Irunlarrea 3, Complejo Hospitalario de Navarra, 31008. Pamplona, Navarra. Spain

[5]Division of Medicine, University College London, London, London, United Kingdom

[6]Department of Molecular and Integrative Physiology, University of Michigan, Ann Arbor, Michigan, United States

[7]Laboratory of Gene Regulation and Signal Transduction, Departments of Pharmacology and Pathology, School of Medicine University of California San Diego, 9500 Gilman Drive, La Jolla, CA 92093, United States

Abstract

Mitogen activated protein kinases (MAPKs) including Erk, Jnk and p38 regulate diverse cellular functions, and are thought to be controlled by independent upstream activation cascades. Here we show that the sestrins bind to and co-ordinate simultaneous Erk, Jnk and p38 MAPK activation in T lymphocytes within a new immune-inhibitory complex (sestrin-MAPK Activation Complex; sMAC). Whereas sestrin ablation resulted in broad reconstitution of immune function in stressed T cells, inhibition of individual MAPKs only allowed partial functional recovery. T cells from old humans and mice were more likely to form the sMAC, and disruption of this complex restored antigen-specific functional responses in these cells. Correspondingly, sestrin deficiency or

*Correspondence: **Arne N Akbar a.akbar@ucl.ac.uk** or **Alessio Lanna alessio.lanna@kennedy.ox.ac.uk**.

simultaneous inhibition of all three MAPKs enhanced vaccine responsiveness in old mice. Thus, disruption of sMAC provides a foundation for rejuvenating immunity during ageing.

Ageing is associated with a substantial decline in immune function that manifests as increased incidence of infection and malignancy and decreased responsiveness to vaccination [1,2]. Given the worldwide demographic shift towards an older age [3], it is essential to understand mechanisms involved with age-related decline of immunity and identify strategies for restoring immune function. Recent studies suggest causative links between immunesenescence, metabolism and ageing and reveal that some of the age-associated decline in immune function may be reversible [4–8]. However, how the myriad of functional defects simultaneously appear in individual aged cells remains largely unknown.

Human T cells that exhibit multiple features of senescence increase during ageing [9]. There is a sequential loss of the costimulatory receptors CD27 and CD28 as T cells progress towards senescence [10]. Early-stage T cells within the CD4 compartment are CD27$^+$CD28$^+$, those at an intermendiate stage are CD27$^-$CD28$^+$, while the senescent T cell population is CD27$^-$CD28$^-$ [5].

Mitogen activated protein kinases (MAPKs) are signal transducing enzymes involved in diverse aspects of mammalian physiology, including senescence, ageing and metabolism [11]. Three main subgroups of MAPKs have been identified: Erk, Jnk and p38 [12]. Given the broad functions they control and the existence of independent upstream activation cascades, it is thought that each MAPK subgroup is separately regulated within individual cells [12–14]. The possibility that all three MAPK subgroups may be co-ordinately controlled within a single cell-type has remained unexplored.

Sestrins, the mammalian products of the *Sesn1*, *Sesn2* and *Sesn3* genes [15–17], are a family of poorly understood stress sensing proteins, that lack obvious catalytic domains and stimulate the activation of AMPK by an as yet unknown mechanism while inhibiting mTORC1 signalling [18]. AMPK is a heterotrimeric protein consisting of the catalytic α subunit and the regulatory β and γ subunits that are activated in response to increased intracellular AMP/ATP ratio [19]. Sestrins have been proposed to inhibit mTORC1 signalling through both AMPK-dependent and independent pathways that involve formation of a complex with the RAGA/B GTPases [18,20–25]. Due to their mTORC1 inhibitory activity, various anti-ageing functions have been ascribed to both the mammalian sestrins and their *Drosophila* counterpart, dSesn [20]. However, a possible role of sestrins in the control of the immune response has not been determined.

In this study, we found that sestrins exhibit pro-ageing activities in T lymphocytes. We identified a sestrin-dependent MAPK activation complex (named sMAC hereafter) in these cells, within which the sestrins simultaneously coordinate the activation of Erk, Jnk and p38. Once activated, each MAPK was found to control a unique functional response. Disruption of the sMAC restored antigen-specific proliferation and cytokine production in T cells from old humans and enhanced responsiveness to influenza vaccination in old mice.

Results

Sestrins are broad regulators of T cell senescence

The sestrins exhibit anti-ageing properties in muscle 20 but the immune related functions of these molecules have not been studied. We examined the expression of sestrin1, sestrin2 and sestrin3 proteins in blood-derived primary human CD4$^+$ T cells from young donors (<40 years old) defined as CD27$^+$CD28$^+$ non-senescent T cells (called T$_{erl}$ hereafter), CD27$^-$CD28$^+$ intermediate T cells (T$_{int}$) and CD27$^-$CD28$^-$CD4$^+$ senescent T cells (T$_{sen}$) as described 5. CD4$^+$ T$_{sen}$ cells expressed significantly higher amounts of sestrin1, sestrin2 and sestrin3 proteins than T$_{erl}$ and T$_{int}$ populations (Fig. 1a,b). We probed the function of endogenous sestrin proteins by transducing activated T$_{sen}$ cells with lentiviral vectors co-expressing a green fluorescent protein (GFP) reporter gene and inhibitory shRNAs to the *SESN1* (shSesn1), *SESN2* (shSesn2) or *SESN3* (shSesn3) genes. A non-silencing shRNA lentiviral vector was used as a control (shCtrl) (Supplementary Fig. 1a-c). Transduction of shSesn1, shSesn2 or shSesn3 in T$_{sen}$ cells resulted in broad functional reversal of senescence, including enhanced cell proliferation (Fig. 1c) and telomerase activity (Fig. 1d), diminished DNA damage foci (Fig. 1e), re-expression of the TCR signalosome components Lck and Zap70 (Fig. 1f and data not shown) and of the co-stimulatory receptors CD27 and CD28 (Fig. 1g) compared to shCtrl transduction. This enhancement of functionality in CD4$^+$ T$_{sen}$ cells was accompanied by restored calcium flux (Fig. 1h) and IL-2 synthesis (Fig. 1i). Therefore, in contrast to their well documented anti-ageing properties in invertebrates[20,26], the sestrins induced multiple characteristics of senescence in T cells.

Sestrins bind to and activate Erk, Jnk and p38 MAPKs in T$_{sen}$ cells

In *Drosophila*, mouse liver homogenates and human embryonic kidney 293 cell lines, sestrin function, including their anti-ageing effects, is largely mTORC1-dependent [20,21,23–25,27,28]. We found that CD4$^+$ T$_{sen}$ cells lacked the expression of both mTOR and its downstream effector kinase S6K1 (Supplementary Fig. 1d). Transduction of shSesn1, shSesn2 or shSesn3 in CD4$^+$ T$_{sen}$ cells restored both mTOR expression and downstream S6K1 activation compared to shCtrl (Supplementary Fig. 1e). However, sestrin-knocked-down CD4$^+$ T$_{sen}$ cells maintained significantly enhanced calcium flux (Supplementary Fig. 1f), IL2 synthesis (Supplementary Fig. 1g), telomerase activity (Supplementary Fig. 1h) and clearance of DNA damage foci (Supplementary Fig. 1i) even in the presence of rapamycin, an mTOR inhibitor, compared to sestrin-knocked down CD4$^+$ T$_{sen}$ cells growth in the absence of rapamycin . This indicates an mTORC1-independent mechanism of sestrin action.

To identify pro-senescence pathways of sestrin action, we immunoprecipitated sestrin1 from blood-derived, unstimulated CD4$^+$ T$_{sen}$ cells using an irrelevant IgG antibody as control. Sestrin1 immunoprecipitates were enriched for phosphorylated Erk, Jnk and p38 MAPKs 12 compared to IgG immunoprecipitation (Fig. 2a). AMPK also precipitated with sestrin1 (Fig. 2a). Similarly, sestrin2 co-immunoprecipitated with phosphorylated Erk, Jnk and p38 MAPKs in CD4$^+$ T$_{sen}$ cells (Supplementary Fig. 2a). This suggests the existence of an endogenous supramolecular sestrin-dependent MAPK activation complex (sMAC), composed of sestrins and phosphorylated AMPK and Erk and Jnk and p38 MAPKs.

Next we measured spontaneous Erk, Jnk and p38 MAPK activation in blood-derived T_{erl} cells, T_{int} cells and T_{sen} cells within the CD4$^+$ subset. Endogenous MAPK activation was enhanced in T_{sen} cells compared to T_{erl} or T_{int} subsets (Supplementary Fig. 2b). To investigate canonical MAPK activators, we probed lysates from T_{erl}, T_{int} and T_{sen} subsets directly *ex vivo* with antibodies to MKK7 (activator of Jnk), MKK4 (activator of Jnk and/or p38) and phosphorylated MEKK1/2 (activator of ERK). T_{sen} cells did not express or endogenously activate any upstream MKK4, MKK7 or MEKK1/2 molecules (Supplementary Fig. 2c). We next transfected siRNAs to MEKK1, MKK7 and MKK4 in T_{erl} and T_{sen} subsets and measured Erk, Jnk and p38 phosphorylation in both cell types by phospho-flow technology. An irrelevant scrambled siRNA was used as control (Supplementary Fig. 2d). Compared to control transfection, silencing MEKK1, MKK7 and MKK4 inhibited Erk, Jnk and p38 phosphorylation in T_{erl} cells, respectively. In contrast, Erk, Jnk and p38 phosphorylation were not affected in T_{sen} cells (Supplementary Fig. 2e). Thus, endogenous MAPK phosphorylation in T_{sen} cells took place in the absence of upstream canonical MAPK signalling 11.

We next investigated whether sestrins are non-canonical regulators of MAPK function. *In vitro* kinase assays demonstrated disrupted MAPK phosphorylation in AMPK immunoprecipitates from CD4$^+$ T_{sen} cells transduced with shSesn vectors compared to shCtrl (Fig. 2b). However, treatment of triple sestrin-silenced T cells with the selective AMPK agonist A-76966229 for 1 hour reconstituted MAPK activation to levels detected per shCtrl transduction (Fig. 2b). We then transduced shAMPK5 and shCtrl vectors in CD4$^+$ T_{sen} cells, immunoprecipitated sestrin2, and performed *in vitro* MAPK assays. MAPK phosphorylation was reduced in sestrin2 immunoprecipitates from shAMPK transduced-CD4$^+$ T_{sen} cells compared to shCtrl (Fig. S2f). Thus, sestrins promoted MAPK activation via AMPK.

Because the Thr-x-Tyr activation loop of MAPK proteins is not a direct AMPK substrate5, we investigated whether sestrin-bound MAPKs undergo AMPK-dependent auto-phosphorylation. Adding exogenous ATP to sestrin1 immunoprecipitates from CD4$^+$ T_{sen} cells strongly enhanced MAPKs phosphorylation in response to incubation with the AMPK agonist A-769662 compared to unstimulated reactions (Fig. 2c). The ATP-competitive Erk inhibitor FR18024, the JNK inhibitor SP-600125 or the p38 inhibitor SB-203580 impeded AMPK agonist-driven MAPK phosphorylation (Fig. 2c). Thus, individual MAPK activities were required for sMAC activation. Furthermore, MAPK auto-phosphorylation was triggered by activation of AMPK.

We next tested whether sestrins modulated MAPK signaling promoting ATP removal from the γ subunit of AMPK28. We therefore transduced CD4$^+$ T_{sen} cells with shSesn vectors either individually or together, then immunoprecipitated AMPKγ, and measured ATP content by ELISA. This progressive single, dual or triple down-regulation of sestrin proteins induced a sestrin-dependent increase in the ATP content of AMPK-γ immunoprecipitates from CD4$^+$ T_{sen} cells compared to shCtrl transduction (Fig. 2d). Likewise, the phosphorylation of AMPK-α, the catalytic subunit of the enzyme, was inhibited in extracts from triple sestrin-knocked-down CD4$^+$ T_{sen} cells compared to shCtrl transduction (Fig. 2e). In addition, when we transfected siRNA to AMPK-γ in CD4$^+$ T_{sen} cells (Supplementary

Fig. 2f) and immunoprecipitated sestrin1, we found reduced Erk, Jnk and p38 MAPK presence in the sestrin1 complex compared to siCtrl transfection (Fig. 2F). Thus, sestrins regulate Erk, Jnk and p38 MAPK auto-phosphorylation by fine-tuning AMPK-γ ATP loading.

Recombinant sestrins reconstitute the sMAC in T$_{erl}$ cells

We performed 'in vitro reconstitution' experiments using lysates from CD4$^+$ (T$_{erl}$ cells), which do not express endogenous sestrin proteins. We transfected siAMPK-γ or siCtrl into T$_{erl}$ cells that were lysed and immunoprecipitated with AMPK-α antibodies 36h later. We then added either recombinant sestrin1/2/3 or GFP proteins and measured Erk, Jnk and p38 phosphorylation. The addition of sestrins triggered a dose-dependent activation of AMPK-associated MAPKs in lysates from siCtrl-transfected CD4$^+$ T$_{erl}$ cells compared to addition of recombinant GFP protein (Fig. 3a). In contrast, siAMPK-γ-transfection in CD4$^+$ T$_{erl}$ cells prevented sestrin-driven MAPK activation (Fig. 3a). MAPK recruitment to AMPK was not significantly altered by recombinant sestrins in these in vitro reconstitution assays (Fig. 3b). These data suggest that sestrins coordinated the sMAC upstream of AMPK-γ and that all MAPKs were bound to AMPK in their inactive form.

To study whether the sMAC formed as a unique complex, we added all three Sestrins to lysates of blood-derived primary human CD4$^+$ T$_{erl}$ cells, then analysed sestrin2 immunoprecipitates using gel-filtration chromatography. Under native conditions, the sMAC eluted with an estimated molecular mass of about 1000 kDA (Fig. 3c), while the sestrin-mTORC1 inhibitory complex, which is known to contain GATOR2 and RAGA/B 23–25, was 660 kDA (Fig. 3c). Similar size endogenous complexes were eluted from lysates obtained from CD4$^+$ T$_{erl}$ cells that had been glucose starved for 12 hours 5 and immunoprecipitated with sestrin2 (not shown), indicating that physiological stress stimuli also triggered the formation of two sestrin-containing complexes of different sizes, controlling either mTORC1 or MAPK activities in primary human T$_{erl}$ cells.

To determine the physiological impact of endogenous sMAC formation in CD4$^+$ T$_{erl}$ cells, we transduced these cells with either all three shSesn1/shSesn2/shSesn3 or shCtrl lentivectors and exposed them to irradiation to induce a stress-response. Sestrin expression was up-regulated in T$_{erl}$ cells after irradiation (Supplementary Fig. 3a). Importantly, Erk, Jnk and p38 phosphorylation was strongly induced upon irradiation in shCtrl-transduced CD4$^+$ T$_{erl}$ cells compared to triple-sestrin-silenced CD4$^+$ T$_{erl}$ cells (Fig. 3d). Notably, triple sestrin-knockdown in irradiated CD4$^+$ T$_{erl}$ cells preserved telomerase activity (Supplementary Fig. 3b) and IL-2 production compared to irradiated shCtrl-transduction (Supplementary Fig. 3c). Sestrin-silenced-T$_{erl}$ cells also showed reduced irradiation-triggered DNA damage (Supplementary Fig. 3d), indicating that sestrin expression was required for induction of senescence in stressed T cells.

Individual MAPKs control distinct aspects of T cell senescence

Because all three MAPKs were activated in the sMAC following AMPK-activation, we investigated the role of each MAPK in this complex. We treated CD4$^+$ T$_{sen}$ with the Erk inhibitor FR18024, the Jnk inhibitor SP-600125 or the p38 inhibitor SB-203580 for 36h

before immunoprecipitating sestrin1 and measuring Erk, Jnk, and p38 phosphorylation. Endogenous MAPK phosphorylation of sestrin1-associated MAPKs was inhibited in MAPKi-treated CD4$^+$ T$_{sen}$ cells compared to DMSO treatment (Supplementary Fig. 4a). In these experiments, blocking any MAPK restored the CD3 and rhIL-2-induced proliferation of CD4$^+$ T$_{sen}$ cells to a similar extent, by 2- to 2.5-fold, compared to DMSO vehicle (Supplementary Fig. 4b). However, only inhibition of p38, but not inhibition of Jnk or Erk, enhanced telomerase activity in CD3/rhIL-2-activated CD4$^+$ T$_{sen}$ cells compared to DMSO (Fig. 4a), as previously reported [4,5,30]. Conversely, blocking Erk, but not p38 or Jnk activation, decreased endogenous DNA damage foci in CD3/rhIL-2-activated CD4$^+$ T$_{sen}$ cells (Fig. 4b). Finally, blocking Jnk, but not p38 or Erk activation reconstituted the expression of both the key TCR signalosome component Lck in CD4$^+$ T$_{sen}$ cells compared to DMSO treatment (Fig. 4c), and that of the co-stimulatory receptor CD28 (not shown). Similar results were obtained when Erk, p38 and Jnk were individually silenced in CD4$^+$ T$_{sen}$ cells (Supplementary Fig. 4c-d). Thus, while MAPKs activation promoted T cell senescence, each MAPK regulated unique functional hallmarks of the senescence programme.

Next we incubated sestrin2-shRNA-transduced CD4$^+$ T$_{sen}$ cells with the AMPK agonist A-769662, which activates AMPK independently of sestrins (Supplementary Fig. 4e) followed by treatment with siRNAs specific for either Erk, p38 and Jnk for 48 hours. Sestrin2 knock down in T$_{sen}$ cells enhanced telomerase activity (Fig. 4d), T cell activation as measured by increased calcium flux (Fig. 4e) and decreased formation of DNA damage foci (Fig. 4f) compared to shCtrl transduction. However the agonist-induced activation of AMPK reversed these functional changes (Fig. 4d-f), suggesting that the sestrins act via AMPK to inhibit functional responses in CD4$^+$ T$_{sen}$ cells. Importantly, transfection of siRNAs to either p38, Jnk or Erk in AMPK agonist-treated, sestrin2-knocked-down CD4$^+$ T$_{sen}$ cells restored telomerase activity and TCR activation and reduced DNA damage foci, respectively (Fig. 4d-f). Similar observations were made when silencing sestrin1 in CD4$^+$ T$_{sen}$ cells (Fig. S4f). Thus, each MAPK in the sMAC controlled different aspects of T cell senescence downstream of a common sestrin trigger.

Enhanced sMAC formation with age

We investigated whether the sestrins preferentially modulate T cell function in older humans. We found up to a 10-fold increase in sestrin expression in total CD4$^+$ T cells from older subjects (70-85 years) compared to younger subjects (20-35 years) (Fig. 5a). Increased sestrin expression was most pronounced within the CD4$^+$ T$_{sen}$ cells from old compared to young individuals (Fig. 5b). We did not detect sMAC in CD4$^+$ T$_{erl}$ cells from younger individuals by image-stream analysis (Fig. 5c and Supplementary Fig. 8a) while sestrin2 co-localized with p-Erk, p-Jnk and p-p38 in CD4$^+$ T$_{sen}$ isolated from the same subjects (Fig. 5c). In contrast, both CD4$^+$ T$_{sen}$ and T$_{erl}$ cells from older humans showed sestrin2 and p-MAPK co-localization, especially in the CD4$^+$ T$_{sen}$ subset (Fig. 5c). Single cell analysis of co-localization scores of sestrin2 and p-MAPKs showed an age-dependent increase in sMAC formation (Fig. 5d). This identifies enhanced formation of the sMAC in human T cells during ageing.

Shingles is caused by the re-activation of varicella zoster virus (VZV) and the incidence of this disease increases during ageing [31,32]. In both young (20-35 years) and old (70-85 years) individuals, the CD4$^+$ T_{erl} cells showed higher proliferative activity in response to VZV antigen activation than the CD4$^+$ T_{sen} population (Fig. 5e). In addition, the proliferation of both subsets was lower in old compared to young individuals (Fig. 5e). ShRNA-mediated silencing of sestrin1 in CD4$^+$ T_{sen} cells from old donors significantly enhanced their proliferation (Fig. 5f) and IL-2 synthesis (Fig. 5g) after VZV activation compared to shCtrl transduction, especially at low antigen dose and when transducing shSesn2 and shSesn3 in addition to shSesn1 (Fig. 5f-g). Similar results were obtained with cytomegalovirus (CMV)-specific T cell responses from old humans (Supplementary Fig. 5a-b). Therefore, silencing of sestrin expression in primary T cell populations from old humans enhanced antigen-specific proliferation and cytokine production *in vitro*.

Sestrin deficiency enhances responsiveness to vaccination in old mice

CD4$^+$ T cells from 20-month old mice showed increased expression of sestrin1, sestrin2 and sestrin3 proteins compared to those from 2-month old animals (Supplementary Fig. 6a). We investigated the response to influenza vaccination in aged-matched *Sesn1$^{+/-}$* and *Sesn1$^{-/-}$* mice. The *Sesn1$^{-/-}$* animals did not express sestrin1 (Supplementary Fig. 6b). These mice were co-housed for 20 months and challenged subcutaneously with FLUAD, a clinically approved trivalent inactivated influenza vaccine that is also effective in rodents [33]. Saline injection served as control. After five days, *Sesn1$^{-/-}$* but not *Sesn1$^{+/-}$* mice exhibited splenomegaly (Supplementary Fig. 6c) and a three-fold increase in splenocytes after vaccination (Fig. 6a). Correspondingly, there was a 2-fold increase in the frequencies of splenic CD4$^+$ and CD8$^+$ T cells in vaccinated *Sesn1$^{-/-}$* mice compared to vaccinated *Sesn1$^{+/-}$* mice (Fig. 6b and Supplementary Fig. 6d). The frequency of myeloid and NK cells were also increased in vaccinated *Sesn1$^{-/-}$* mice compared to controls by 5 and 2-fold respectively (Supplementary Fig. 6e,f). Within the CD4$^+$ T cell compartment, there was a 2-fold expansion of CD62L$^-$CD44$^+$ T effector cells and a corresponding contraction of the CD62L$^+$CD44$^-$ naïve T cell population from vaccinated *Sesn1$^{-/-}$* mice compared to vaccinated *Sesn1$^{-/+}$* controls (Supplementary Fig. 6g). These differences in T cell frequencies between genotypes were not evident before vaccination (not shown). Functionally, *Sesn1$^{-/-}$* CD4$^+$ T cells exhibited increased IL-2 and IFN-γ production and enhanced proliferation compared to vaccinated *Sesn1$^{-/+}$* controls after vaccination (Fig. 6d,e). Therefore, sestrin deficiency enhances T cell responsiveness and also the expansion of innate cells during ageing *in vivo*.

To investigate whether enhanced T cell responsiveness after vaccination was antigen-specific, we re-challenged *Sesn1$^{+/-}$* or *Sesn1$^{-/-}$* T cells with *Sesn1$^{+/-}$* antigen presenting cells (APCs) pulsed with FLUAD *in vitro*. There was increased IFN-γ and IL-2 synthesis *by Sesn1$^{-/-}$*, compared to *Sesn1$^{+/-}$* CD4$^+$ T cells (Fig. 6f and data not shown). In addition, siRNA-mediated silencing of sestrin2 in *Sesn1$^{-/-}$* null CD4$^+$ T cells further increased their responsiveness to *Sesn1$^{+/-}$* APCs pulsed with FLUAD (Fig. 6f).

When measuring antibody titres, we found a 2-to-3-fold increase in influenza-specific circulating IgGs in *Sesn1$^{-/-}$* compared to *Sesn1$^{+/-}$* mice (Fig. 6g) and *Sesn1$^{-/-}$* B cells showed

indeed enhanced IgG isotypic switch compared to *Sesn1*^{+/-} mice after vaccination (Supplementary Fig. 6h). B cell frequencies, however, were slightly reduced in the spleen of vaccinated *Sesn1*^{-/-} mice compared to vaccinated *Sesn1*^{+/-} controls (not shown). The collated data on the increase in numbers of all cell types examined before and after vaccination are shown in Supplementary Fig. 6i. Thus, sestrin deficiency restored vaccine responsiveness during ageing *in vivo*.

MAPK inhibition phenocopies sestrin deficiency *in vivo*

We next measured Erk, Jnk and p38 phosphorylation in sestrin2^{+} CD4^{+} T cells which comprised up to 70% of the total CD4^{+} T cell pool (Fig. 7a) from 20-month old *Sesn1*^{-/+} and *Sesn1*^{-/-} mice after FLUAD vaccination. Erk, Jnk and p38 phosphorylation was robust in sestrin2^{+} CD4^{+} T cells from *Sesn1*^{-/+} mice, and reduced in *Sesn1*^{-/-} CD4^{+} T cells (Fig. 7b). Notably, reduced Erk, Jnk, and p38 phosphorylation and increased IFN-γ production correlated directly in sestrin2^{+} CD4^{+} T cells from vaccinated *Sesn1*^{-/-} mice compared to vaccinated *Sesn1*^{-/+} mice (Fig. 7c). Sestrin1 deficiency did not affect Erk, Jnk and p38 phosphorylation in the minor Sestrin2^{-} CD4^{+} T cells compared to those from *Sesn1*^{-/+} mice (Supplementary Fig. 7a). To test whether inhibition of all MAPKs would boost vaccine responsiveness in aged mice, we administered the Erk inhibitor FR18024, the Jnk inhibitor SP-600125 and the p38 inhibitor SB-203580 by intra-peritoneal injection either individually or together to 16-month old mice vaccinated with FLUAD, and examined both the sestrin2^{+} CD4^{+} T cell and CD19^{+} B cell subsets. Mice treated with all three MAPK inhibitors developed splenomegaly (Fig. 7d and Supplementary Fig. 7b) and showed increased splenic CD4^{+} T cell numbers compared to DMSO vehicle controls or mice receiving the individual MAPK inhibitors after vaccination (Fig. 7e). MAPK self-phosphorylation was either selectively or globally inhibited in CD4^{+} T cells from mice treated with either individual MAPK inhibitors or all of them together respectively compared to DMSO (Fig. 7f). Triple, but not individual inhibition of MAPKs boosted IFN-γ synthesis in sestrin2^{+} CD4^{+} T cells following vaccination compared to DMSO-treatment (Fig. 7g). Triple MAPK inhibition also induced a 3-fold increase in the frequencies of sestrin2^{+} CD19^{+} B cells undergoing vaccine-specific IgG-isotypic switch compared to DMSO, which was not observed when inhibiting individual MAPKs (Fig. 7g). In contrast, inhibition of MAPK signaling in both sestrin2^{-} CD4^{+} T and CD19^{+} B cells reduced vaccine-induced IFN-γ production and IgG-isotypic switch, respectively (Supplementary Fig. 7c). Thus, disruption of all MAPK pathways in Sestrin2^{+} T and B cell populations enhanced vaccine responsiveness in old mice.

The sMAC is formed in mouse T cells

We isolated CD4^{+} T cells from *Sesn1*^{-/+} and *Sesn1*^{-/-} mice, immunoprecipitated sestrin2, and investigated Erk, Jnk and p38 phosphorylation. Sestrin2 complexes from *Sesn1*^{-/-} CD4^{+} T cells showed reduced p-Erk, p-Jnk and p-p38 than those from *Sesn1*^{-/+} CD4^{+} T cells (Fig. 8a-b). Sestrin2-MAPK binding was not affected by sestrin1 deficiency (not shown). Image-stream analysis confirmed disrupted sMAC activation in spleen-derived CD4^{+} T cells from *Sesn1*^{-/-} mice compared to *Sesn1*^{+/-} mice (Fig. 8c-d). *In vitro* kinase assays showed that incubation of sestrin2 immunoprecipitates from *Sesn1*^{-/-} mouse CD4^{+} T cells with recombinant human sestrin1 protein reconstituted MAPK activation in lysates from these cells (Fig. 8e). This effect was not observed in sestrin2 immunoprecipitates from AMPK-γ

silenced CD4^{+} T cells compared with siCtrl transfection (Fig. 8e). The A-769662 agonist-driven activation of AMPK also restored MAPK phosphorylation in sestrin2 immunoprecipitates from splenic *Sesn1*^{-/-} CD4^{+} T cells, compared to DMSO treatment, and was further enhanced by the addition of ATP, needed to fuel MAPK auto-phosphorylation (Fig. 8f). Thus, the sMAC was also formed and coordinated by the sestrins in mice.

Discussion

Here we show that in T_{sen} cells Erk, Jnk and p38 MAPK are simultaneously activated due to constitutive expression of sestrin proteins. In flies, sestrin expression increases upon maturation and ageing and triggers feedback anti-ageing pathways through a TORC1 inhibitory complex 20. Similarly, in muscle, sestrins exhibit mTORC1-dependent anti-ageing activities 22. We now describe an opposite pro-ageing function of sestrins in T cells that occurred independently of mTORC1, and instead was mediated by an Erk/Jnk/p38 MAPK activation complex (sMAC). Such co-ordinated MAPK activation was previously unknown and is distinct from the canonical MAPK activation cascades where Erk, Jnk and p38 are regulated independently 11.

All regulatory elements within the sMAC interacted constitutively in T_{sen} cells. The sMAC was also distinct from the previously described sestrin-mTORC1 inhibitory complexes containing GATOR and RAG proteins 23–25, suggesting that the anti-ageing/pro-ageing dichotomy of sestrin action in T cells versus other cell types may depend on different sestrin-protein interactions. Consistently, mTORC1 inhibition has been strongly associated with longevity in both muscle and insects 34 while p38 MAPK activation can drive T cell ageing and senescence 4–6,30 . Sestrin may therefore exert anti- or pro-ageing effects through two different macromolecular complexes. Whether the sMAC also controls ageing in non-immune cells remains to be determined.

The sMAC also formed in T_{erl} cells upon glucose deprivation (not shown), and this extends previous observations highlighting the convergence of both senescence and low-nutrient signals to regulate T cell function ('Intra-sensory' signalling) 5,9. When examining glucose deprived sestrin-silenced T_{erl} cells, we also found disrupted AMPK phosphorylation and a transient increase in T cell activation followed by T cell death if glucose deprivation persisted (not shown). Sestrins may thus function as an energy-sensing 'rheostat' that directly binds to AMPK-γ and promotes AMPK activation to favour T cell survival at the expenses of function under severe stress.

The sMAC was larger than the sestrin-mTORC1 inhibitory complex, and additional unknown proteins may contribute to its regulation. p38 auto-phosphorylation was a feature of non-canonical MAPK activation in T cells which requires p38 binding to specific scaffolding molecules such as TAB1 5,35. We now show that sMAC coordinates the simultaneous activation of all MAPK pathways. However, TAB1 was not required for the activation of Jnk or Erk, while it mediated activation of p38 within the sMAC (not shown). We propose a model in which three separate MAPK sub-complexes are constitutively bound to AMPK in their inactive form. When expressed, sestrins would promote the unloading of ATP from AMPK-γ and activate the AMPK complex. In turn, this would trigger the auto-

phosphorylation of all associated MAPKs. Distinct scaffolding molecules may be required to support the auto-phosphorylation of each of the 3 MAPKs in the sMAC.

Silencing of sestrin expression allowed a broad enhancement of T cell activity, whereas downstream targeting of any individual MAPK was much more selective. It is therefore possible to exert narrower or broader control over senescence-related T cell functional changes by targeting different molecules within the sMAC. Since each MAPK controlled different aspects of T cell senescence, they may have to be simultaneously targeted for effective immune boosting during ageing. However, direct inhibition of MAPKs may not be feasible for immunotherapy as it would negatively regulate the responses of T and B-lymphocytes that do not express sestrins. On the other hand, inhibition of the sestrins would disrupt global MAPK signalling. This would spare sestrin-negative cells, in which MAPKs may be activated via canonical pathways 36 and may thus circumvent toxicity. A caveat to consider is that sestrin inhibition may enhance the proliferative activity of senescent cells that have residual DNA damage and therefore, prolonged inhibition of sestrins may result in malignancy 37. However, short-term inhibition of sestrins could be a beneficial immunotherapeutic strategy.

Methods

Human studies

We collected heparinized peripheral blood samples from 120 individuals (aged 20-85, male 55% and female 45%). Samples from young (aged: 20-35) and old (aged: 65-80) donors were obtained with the approval of the Ethical Committee of Royal Free and University College Medical School and voluntary informed consent, in accordance with the Declaration of Helsinki. Donors did not have any co-morbidity, were not on any immunosuppressive drugs, and retained physical mobility and lifestyle independence.

Western Blot analysis

Lysates from 2×10^6 cells were used for Western Blot analysis. Endogenous signaling studies were assessed in *ex vivo* purified CD4^{+} CD27/CD28 T cell subsets as described previously5. Transduced CD4^{+} CD27^{-} CD28^{-} T cells were analyzed by immunoblotting one week after activation (see below). Membranes were probed with antibodies to: Sestrin1 (Genetex; Abcam), Sestrin2 (Cell Signaling), Sestrin3 (Sigma), ERK, p-ERK, p-JNK, p-p38, AMPK-α, p-AMPK-α, mTOR S6K1, MKK7, MKK4, p-MEK1/2 and GAPDH (all from Cell Signaling).

Immunoprecipitation

For co-immunoprecipitation analysis, cell-lysates were prepared using ice-cold HNGT buffer (50 mM HEPES, pH 7.5, 150 mM EDTA, 10 mM sodium pyrophosphate, 100 mM sodium orthovanadate, 100 mM sodium fluoride, 10 mg/ml aprotinin, 10 mg/ml leupeptin, and 1 mM phenylmethylsulfonyl fluoride). Lysates from 20×10^6 cells were used for immunoprecipitation analysis. For the minor CD4^{+} CD28^{−} CD27^{−} subset, cells from two separate individuals were pooled to obtain sufficient material for the assay. Extracts were incubated with the indicated antibodies at 4 °C on a rotary shaker overnight, followed by

incubation with protein A–G conjugated agarose beads (Santa Cruz Biotechnology) at 4 °C for 3 h. Samples were washed and analyzed by immunoblotting as indicated. Co-immunoprecipitated proteins were detected using Mouse Anti-rabbit IgG Conformation Specific (L27A9; Cell Signalling) or Mouse Anti-rabbit IgG light chain, followed by a secondary anti-mouse IgG antibody (all from Cell Signalling) and ECL Prime Western detection kit (GE Healthcare).

In vitro binding assay

Briefly, lysates from $CD4^+$ $CD27^+$ $CD28^+$ T cell were incubated with recombinant Sestrins for 1 hour, followed by phosphorylated or total AMPK immunoprecipitation. AMPK complexes were washed extensively and global MAPK activation was measured by immunoblotting or *in vitro* kinase assays (see below). Absolute MAPK binding was determined using ELISA-based total ERK, JNK and p38 detection assays according to the manufacturer's instructions (Abcam; see below). In some experiments, absolute MAPK binding was determined on endogenous Sestrin immunoprecipitates from $CD4^+$ $CD27^-$ $CD28^-$ T cells, 48h post-transfection. MAPK binding assays are shown as proportional to fold increase at 450 nm absorbance emission of triplicate wells ± s.e.m, and were normalized to the indicated 'bait' proteins i.e. Sestrin1 (MBS9327570) or AMPK-α (ab151280) used in the immunoprecipitation assay.

In vitro kinase assay

Sestrin or AMPK Immunoprecipitates were washed twice in lysis buffer and twice in kinase buffer (all from Cell Signaling). Kinase reactions were incubated for 30 min at 30 °C either in the absence or in the presence of 200 μM ATP (Cell Signaling), as indicated. MAPK activity was assessed using Phospho-Tracer ELISA Kits according to the manufacturer's instructions (Abcam; see below). In some experiments, exogenous recombinant human Sestrin proteins (Genway; 1 μg/mL), the AMPK agonist A-769662 (150 μM), the Erk inhibitor FR18024 (20 μM); the Jnk inhibitor SP-600125, (10 μM); or the p38 inhibitor SB-203580, (10 μM) were added directly to the *in vitro* kinase reaction itself for 30', as indicated. *In vitro* kinase assays are shown as proportional to fold increase at 450 nm absorbance emission of triplicate wells ± s.e.m, normalized to the total amounts of co-immunoprecipitated MAPKs.

Detection of co-immunoprecipitated proteins by ELISA

Briefly, an antibody mix was prepared by adding Capture Antibody Reagent(s) to MAPKs and Detection Antibody Reagent (both provided with the Phospho Tracer kit by Abcam), in a 1:1 ratio, and 50 μl of this antibody mix were added to the *in vitro* kinase/binding reaction product (50 μl), loaded in the Phospho Tracer micro-plates. Antibody binding was then allowed for 1 hour at room temperature on a micro-plate shaker. Wells were rinsed three times with 200 μl of 1 X washing buffer (provided with the kit). Meanwhile, a substrate mix was prepared, immediately before use, by diluting 1:100 the HR-substrate 10-Acetyl-3, 7-dihydroxyphenoxazine (ADHP) with ADHP Dilution Buffer (both provided with the kit), a stabilized $H2O2$ solution. Next, 100 μl of this substrate mix were added to each well, and incubated 10' at room temperature on a micro-plate shaker for colour development. The reaction of conversion of ADHP into the fluorescent molecule Resorufin was then stopped

by adding 10 μl of stop solution to each well. Signal was read using an Elisa reader micro-plate. Background was calculated in parallel IgG control immunoprecipitation reactions.

Measurement of AMPK-γ ATP loading

T cell AMPK-γ 1 immunoprecipitates were analyzed for ATP content using an ATP determination kit, according to the manufacturer's instructions (Life Technologies). Total AMPK-γ 1 immunoprecipitates were quantified by Elisa (LifeSpan Biosciences).

T cell activation dynamics

For detection of intracellular calcium, we used x-Rhod1, a visible light-excitable calcium chelator suitable for flow-cytometry. Briefly, transduced cells were incubated with this dye (2.5 μM, 37C; 20') washed in indicator-free medium to eliminate unspecific binding, then incubated for further 30 mins to allow complete dye de-esterification, as instructed by the manufacturer (Molecular Probes, Invitrogen). Cells were then stimulated by aCD3 for 2 mins immediately followed by flow-cytometry analysis. In experiments with 'multi-layer' modulation of signaling, stably-transduced primary human CD27⁻ CD28⁻ CD4⁺ T cells were activated with α-CD3 (0.5 μg/mL) and rh-IL2 (10 ng/mL) for 24 hours in the presence of the indicated siRNAs and/or the AMPK-activator A-769662 (150 μM) or the m-TORC1 inhibitor rapamycin (20 ng/mL), followed by dye incubation, short-term re-activation and intracellular calcium detection, as above. IL-2 synthesis or release was analyzed by ELISA-based or intra-cellular flow cytometry respectively, as indicated. Active cycling upon stimulation was further confirmed by staining for the proliferation-related antigen ki-67.

Lentiviral vector design

The pHIV1-SIREN-GFP system used for knockdown of gene expression possesses a U6-shRNA cassette to drive shRNA expression and a GFP reporter gene which is controlled by a PGK promoter5. The following siRNA sequences were used for gene knockdowns: CCTAAGGTTAAGTCGCCCTCG (shCTRL), ATGATGTCAGATGGTGAATTT (shAMPKα), CCAGGACCAATGGTAGACAAA (shSesn1), CCGAAGAATGTACAACCTCTT (shSesn2) and CAGTTCTCTAGTGTCAAAGTT (shSesn3). The shAMPKα sequence was previously described and validated in primary human CD4⁺ T cells5. VSV-g pseudotyped lentiviral particles were produced, concentrated and titrated in HEK 293 cells as described38.

Cell cultures and lentiviral transduction of primary human T lymphocytes

Cells were cultured in RPMI 1640 medium supplemented with 10% heat-inactivated FCS, 100 U/ml penicillin, 100 mg/ml streptomycin, 50 μg/ml gentamicin, and 2 mM L-glutamine (all from Invitrogen) at 37°C in a humidified 5% CO_2 incubator. Purified human highly differentiated CD4⁺ CD27⁻ CD28⁻ T cells were activated in the presence of plate-bound αCD3 Ab (purified OKT3, 0.5 μg/ml) plus rhIL-2 (R&D Systems, 10 ng/ml), and then transduced with pHIV1-Siren lentiviral particles (MOI=10) at 48 and 72 hours after activation. Non-senescent CD4⁺ CD27⁺ CD28⁺ T cells were cultured and transduced as above after activation by plate-bound αCD3 (0.5 μg/mL) plus αCD28 (0.5 μg/mL). When antigen specific responsiveness was assessed, CD27⁻ CD28⁻ CD4⁺ T cells were re-activated

10 days post-transduction using autologous antigen presenting cells (APCs) pre-loaded for 4 hours with various dilutions of Varicella zoster virus lysates (Zeptometrix Corporation), as indicated. Antigen presenting cells were obtained by depleting CD3 positive cells from autologous, fresh PBMC preparations and cultured with transduced T cells, in a 3:1 ratio. Antigen-specific responses are shown as fold increase normalized to transduced cells before re-stimulation, with control cells set as 1, in triplicate experiments.

Transfections

Human or mouse primary CD4$^+$ T cells were transfected with siRNAs to Erk, Jnk, p38, AMPK-γ, MEKK1, MEKK4, MEKK7 or an irrelevant control siRNA sequence (all from Santa Cruz Biotechnology) using Nucleofector Kit according to the supplier's protocol (Amaxa, Lonza Walkersville; program V024), as indicated. Cells were then rested and analyzed 48 hours later for functional or signaling readouts.

Quantitative PCR (Real time analysis)

Four days post transduction, samples from 5 x 10^5 viable senescent CD4$^+$ CD27$^-$ CD28$^-$ T cells were resuspended in TRIzol (Ambion). For cDNA synthesis, RNA was retro-transcribed using M-MuLV Reverse Transcriptase (New England Biolab) and random primers. Relative transcript expression was normalized using the CT threshold cycle method according to the supplier's protocol (Applied Biosystems).

Signaling studies

Cells were fixed with warm Cytofix Buffer (BD Biosciences) at 37°C for 10 min, permeabilized with ice-cold Perm Buffer III (BD Biosciences) at 4°C for 30 min and then incubated for 30 min at room temperature with antibodies to: LCK, ZAP-70, p-AMPK, Sestrin2 (all from Cell Signalling), PercPCy5-conjugated p-Erk, Alexa-Fluor 647-conjugated p-Jnk, PE-conjugated p-p38 and PE-conjugated γ-H2A-x (all from BD Biosciences). When primary unconjugated antibodies were used, they were subsequently probed with a secondary mouse (or goat) Alexa Fluor 647-conjugated anti-rabbit IgG (BD Biosciences) for 30' at room temperature, in the dark. After washing in Stain Buffer (BD Pharmingen), samples were analysed immediately using an LSR Fortessa (BD Biosciences). Data were analyzed using FlowJo software (Treestar). For transduced cells, events were gated on the GFP$^+$ compartment as indicated.

Measurement of telomerase activity

Telomerase activity was determined using the TeloTAGGG telomerase ELISA kit from Roche according to the manufacturer's instructions from extracts of 2 x 10^3 viable CD4$^+$ CD27$^-$ CD28$^-$ T cells. The absolute numbers of CD4$^+$ CD27$^-$ CD28$^-$ T cells were enumerated by trypan blue (Sigma) and proliferation was determined by Ki67 staining as described 39. Telomerase activity is expressed as proportional to fold increase at 450 nm absorbance emission of triplicate wells ± s.e.m.

Proliferation assays

Four days post transduction, proliferation of activated senescent human CD27$^-$ CD28$^-$ CD4$^+$ T cells was assessed by overnight probing with [^{3}H] thymidine and expressed as fold increase in [^{3}H] thymidine incorporation (cpm) of triplicate wells ± s.e.m. Alternatively, antigen-specific responsiveness of senescent human CD27$^-$ CD28$^-$ CD4$^+$ T cells was assessed by staining for the cell cycle related nuclear antigen Ki-67 four days post-activation with autologous VZV-pulsed APCs.

Mice

Sesn1$^{-/-}$ mice were generated from Sesn1$^{+/-}$ embryonic stem (ES) cells in the C57BL/6 background, obtained from EUCOMM. These cells were created by targeted gene trap approach and contain reporter-tagged insertion within intron 5 of the Sesn1 gene with a strong splice acceptor site expressing a β-Gal-Neo fusion protein that disrupts the Sesn1 ORF. The Sesn1$^{+/-}$ mice, produced from ES cells, were backcrossed again to wild-type C57BL/6 mice (n = 5) to eliminate any non-specific genetic aberrations that may present in the chromosomes from the ES cells. After the backcrossing, the Sesn1$^{+/-}$ mice were interbred to generate Sesn1$^{-/-}$ mice, which were found to be fully viable and fertile. Sesn1$^{+/-}$ littermates were used as a control strain, and co-housed with the Sesn1$^{-/-}$ mice throughout the course of aging experiments. The absence of Sestrin1 mRNA and protein was confirmed by RT-PCR and immunoblot analyses of splenocytes (Fig. S6) as well as other tissues (data not shown). Mice were maintained in filter-topped cages and were given free access to autoclaved chow diet and water, according to National Institutes of Health (NIH) and institutional guidelines. All animal ageing studies were overseen by the University Committee on Use and Care of Animals (UCUCA) at the University of Michigan.

Mouse studies

Age-matched (20 month-old) mice were imported from the University of Michigan, rested for 10 days, and then used for *in vivo* studies. Control Sesn1$^{+/-}$ and Sesn1$^{-/-}$ null mice were subcutaneously injected with the seasonal influenza vaccine FLUAD (Novartis; 1: 20 of the human dose). A saline solution (PBS) was used as control injection. Five days later, animals were euthanized in a CO_2 chamber, spleens collected, and processed for splenocyte isolation. Mouse CD4$^+$ T cells were obtained from splenocytes by immunomagnetic separation (Miltenyi Biotec) and immediately analyzed for phenotypic, signaling and functional profiles by either flow cytometry or Image-Stream, as indicated. CD4$^+$ phenotypic analysis was performed by surface staining to CD62L and CD44. For recall-responses, control Sesn1$^{+/-}$ and Sesn1$^{-/-}$ null CD4$^+$ T cells were re-challenged with control Sesn1$^{+/-}$ APCs pre-loaded with FLUAD (1:100, 1:50 and 1:25 of the human dose), then IL-2$^+$, IFN-γ$^+$ **or•ki67**$^+$ T cells were analyzed 18-hours later by flow-cytometry. All *in vivo* studies were undertaken at University College London in collaboration with Prof. Derek Gilroy (licence no. 70/7354).

Antibody titration

Sesn1$^{+/-}$ and Sesn1$^{-/-}$ mice were vaccinated with FLUAD as above described. One week later, mice were sacrificed and blood samples were immediately collected by cardiac

bleeding. Levels of circulating immunoglobulins (IgGs) were analyzed using a serum dilution of 1:200 in 0.1% non-fat dry milk 0.5% Tween-20/PBS, as described 33. Samples were incubated on Nunc Maxisorp plates pre-coated with FLUAD overnight (1:40; for 18 hours at 4 °C), or PBS as background control. Plates were washed 3 times with 0.5% Tween-20/PBS and blocked with 200 μl of 4% non-fat dry milk (GE-Healthcare). Antigen-specific serum antibodies were detected using horseradish peroxidase (HRP) conjugated antibodies (anti-mouse IgG, Sigma Aldrich) at 1:3000 dilution in 0.1% non-fat dry milk 0.5% Tween-20/PBS, at room temperature. Substrate activity was detected using 100 μL of tetramethylbenzidine (TMB) substrate (BD Biosciences) and stopped using 50 μL 2N H_2SO_4 per well. Circulating vaccine-speciific IgG levels were determined by ELISA (absorbance emission at 450 nm) of triplicate wells ± s.e.m.

Inhibition of Sestrin-MAPK signaling *in vivo*

Aged-matched mice (16 months) were injected i.p. with the Erk inhibitor FR18024 (25 mg/Kg); the Jnk inhibitor SP-600125 (16 mg/Kg); and the p38 inhibitor SB-203580 (10 mg/Kg) individually or with all 3 inhibitors together. Drug vehicle was DMSO. Three hours later, mice were vaccinated with FLUAD as above. Triple and individual MAPK inhibition treatments were then repeated daily. Five days later, mice were culled, spleens collected and the impact of *in vivo* blocking MAPK signaling on immune-responsiveness was analysed in Sestrin2^{+} T and B cell populations, as indicated.

Analysis of the Sestrin-MAPK signalling complex *in vivo*

Primary human or mouse CD4^{+} T cells were fixed with 2% paraformaldehyde, permeabilized with methanol and stained for Sestrin2, p-ERK, p-JNK and p-p38 direclty *ex vivo,* as above described. For human experiments, CD4^{+} T cells were separated into early-differentiated and highly differentiated populations according to their relative CD27/CD28 expression profile from either young (20-35 years) or old donors (70-85 years). All samples were run on an Amnis® Image Stream cytometer using INSPIRE® software, magnification 60x. Data were analyzed using IDEAS® v.6.1 software (Amnis). Co-localization signals were determined on a single cell basis using Bright Detail Similarity (BDS) Score analysis. Co-localization was considered with BDS of 2.0.

Gel-Filtration Chromatography

A Superdex 200 (GE Healthcare) gel filtration column was first equilibrated with 1.5 CV of endotoxin free PBS (Hyclone) at room temperature. Sestrin2 complexes were injected at time 0 (500 ul) and eluted using a single isocratic wash, fractions collected, and analyzed by ELISA-based binding assays (absorbance at 450 nm) across the spectrum for the indicated proteins. Phosphorylated MAPKs were detected using Phospho-Tracer ELISA kits (Abcam) as above described. For detection of Mios (MBS9330396); RagA (MBS9334409); and RagB (MBS9318748). The column was calibrated with protein markers as described 18

Statistical analysis

Graphpad Prism was used to perform statistical analysis. For pairwise comparisons, a paired Student's *t*-test was used. For three matched groups, a one-way analysis of variance

(ANOVA) for repeated measures with a Bonferroni post-test correction was used. $*p<0.05$, $**p<0.01$ and $***p< 0.001$ throughout. For correlation studies, Pearson correlation test.

Data availability

The data generated or analysed during this study are included in this published article and its supplementary information files. The data not shown can be obtained from the corresponding authors upon reasonable request.

Supplementary Material

Refer to Web version on PubMed Central for supplementary material.

Acknowledgements

References

1. Montecino-Rodriguez E, Berent-Maoz B, Dorshkind K. Causes, consequences, and reversal of immune system aging. J Clin Invest. 2013; 123:958–65. [PubMed: 23454758]

2. Dorshkind K, Montecino-Rodriguez E, Signer RAJ. The ageing immune system: is it ever too old to become young again? Nat Rev Immunol. 2009; 9:57–62. [PubMed: 19104499]

3. Lutz W, Sanderson W, Scherbov S. The coming acceleration of global population ageing. Nature. 2008; 451:716–9. [PubMed: 18204438]

4. Di Mitri D, et al. Reversible senescence in human CD4+CD45RA+CD27- memory T cells. J Immunol. 2011; 187:2093–100. [PubMed: 21788446]

5. Lanna A, Henson SM, Escors D, Akbar AN. The kinase p38 activated by the metabolic regulator AMPK and scaffold TAB1 drives the senescence of human T cells. Nat Immunol. 2014; 15:965–72. [PubMed: 25151490]

6. Henson SM, et al. p38 signaling inhibits mTORC1-independent autophagy in senescent human CD8$^+$ T cells. J Clin Invest. 2014; 124:4004–16. [PubMed: 25083993]

7. Li G, et al. Decline in miR-181a expression with age impairs T cell receptor sensitivity by increasing DUSP6 activity. Nat Med. 2012; 18:1518–1524. [PubMed: 23023500]

8. Müller-Durovic B, et al. Killer Cell Lectin-like Receptor G1 Inhibits NK Cell Function through Activation of Adenosine 5'-Monophosphate–Activated Protein Kinase. J Immunol. 2016; 197:2891–2899. [PubMed: 27566818]

9. Akbar AN, et al. Senescence of T Lymphocytes: Implications for Enhancing Human Immunity. Trends Immunol. 2016; 37:866–876. [PubMed: 27720177]

10. Weng N-P, Akbar AN, Goronzy J. CD28(-) T cells: their role in the age-associated decline of immune function. Trends Immunol. 2009; 30:306–12. [PubMed: 19540809]

11. Chang L, Karin M. Mammalian MAP kinase signalling cascades. Nature. 2001; 410:37–40. [PubMed: 11242034]

12. Johnson GL, Lapadat R. Mitogen-activated protein kinase pathways mediated by ERK, JNK, and p38 protein kinases. Science. 2002; 298:1911–2. [PubMed: 12471242]

13. Liu Y, Shepherd EG, Nelin LD. MAPK phosphatases--regulating the immune response. Nat Rev Immunol. 2007; 7:202–12. [PubMed: 17318231]

14. Chen RE, Thorner J. Function and regulation in MAPK signaling pathways: lessons learned from the yeast Saccharomyces cerevisiae. Biochim Biophys Acta. 2007; 1773:1311–40. [PubMed: 17604854]

15. Budanov AV, et al. Identification of a novel stress-responsive gene Hi95 involved in regulation of cell viability. Oncogene. 2002; 21:6017–31. [PubMed: 12203114]

16. Peeters H, et al. PA26 is a candidate gene for heterotaxia in humans: identification of a novel PA26-related gene family in human and mouse. Hum Genet. 2003; 112:573–80. [PubMed: 12607115]

17. Velasco-Miguel S, et al. PA26, a novel target of the p53 tumor suppressor and member of the GADD family of DNA damage and growth arrest inducible genes. Oncogene. 1999; 18:127–37. [PubMed: 9926927]

18. Budanov AV, Karin M. p53 target genes sestrin1 and sestrin2 connect genotoxic stress and mTOR signaling. Cell. 2008; 134:451–60. [PubMed: 18692468]

19. Hardie DG, Ross FA, Hawley SA. AMPK: a nutrient and energy sensor that maintains energy homeostasis. Nat Rev Mol Cell Biol. 2012; 13:251–62. [PubMed: 22436748]

20. Lee JH, et al. Sestrin as a feedback inhibitor of TOR that prevents age-related pathologies. Science. 2010; 327:1223–8. [PubMed: 20203043]

21. Lee JH, et al. Maintenance of metabolic homeostasis by Sestrin2 and Sestrin3. Cell Metab. 2012; 16:311–21. [PubMed: 22958918]

22. Lee JH, Budanov AV, Karin M. Sestrins orchestrate cellular metabolism to attenuate aging. Cell Metab. 2013; 18:792–801. [PubMed: 24055102]

23. Parmigiani A, et al. Sestrins inhibit mTORC1 kinase activation through the GATOR complex. Cell Rep. 2014; 9:1281–91. [PubMed: 25457612]

24. Peng M, Yin N, Li MO. Sestrins Function as Guanine Nucleotide Dissociation Inhibitors for Rag GTPases to Control mTORC1 Signaling. Cell. 2014; 159:122–133. [PubMed: 25259925]

25. Chantranupong L, et al. The Sestrins Interact with GATOR2 to Negatively Regulate the Amino - Acid - Sensing Pathway Upstream of mTORC1. 9 Figure S1.

26. Yang Y-L, et al. SESN-1 is a positive regulator of lifespan in Caenorhabditis elegans. Exp Gerontol. 2013; 48:371–9. [PubMed: 23318476]

27. Chen CC, et al. FoxOs Inhibit mTORC1 and Activate Akt by Inducing the Expression of Sestrin3 and Rictor. Dev Cell. 2010; 18:592–604. [PubMed: 20412774]

28. Hay N. p53 strikes mTORC1 by employing sestrins. Cell Metab. 2008; 8:184–5. [PubMed: 18762019]

29. Goransson O, et al. Mechanism of Action of A-769662, a Valuable Tool for Activation of AMP-activated Protein Kinase. J Biol Chem. 2007; 282:32549–32560. [PubMed: 17855357]

30. Lanna A, et al. IFN-α inhibits telomerase in human CD8^{+} T cells by both hTERT downregulation and induction of p38 MAPK signaling. J Immunol. 2013; 191:3744–52. [PubMed: 23997212]

31. Oxman MN, et al. A vaccine to prevent herpes zoster and postherpetic neuralgia in older adults. N Engl J Med. 2005; 352:2271–84. [PubMed: 15930418]

32. Levin MJ. Immune senescence and vaccines to prevent herpes zoster in older persons. Curr Opin Immunol. 2012; 24:494–500. [PubMed: 22857823]

33. Oh JZ, et al. TLR5-mediated sensing of gut microbiota is necessary for antibody responses to seasonal influenza vaccination. Immunity. 2014; 41:478–92. [PubMed: 25220212]

34. Johnson SC, Rabinovitch PS, Kaeberlein M. mTOR is a key modulator of ageing and age-related disease. Nature. 2013; 493:338–45. [PubMed: 23325216]

35. Round JL, et al. Scaffold protein Dlgh1 coordinates alternative p38 kinase activation, directing T cell receptor signals toward NFAT but not NF-kappaB transcription factors. Nat Immunol. 2007; 8:154–161. [PubMed: 17187070]

36. Ashwell JD. The many paths to p38 mitogen-activated protein kinase activation in the immune system. Nat Rev Immunol. 2006; 6:532–40. [PubMed: 16799472]

37. Akbar AN, Henson SM. Are senescence and exhaustion intertwined or unrelated processes that compromise immunity? Nat Rev Immunol. 2011; 11:289–95. [PubMed: 21436838]

38. Escorts D, et al. Targeting dendritic cell signaling to regulate the response to immunization. Blood. 2008; 111:3050–61. [PubMed: 18180378]

39. Plunkett FJ, et al. The Loss of Telomerase Activity in Highly Differentiated CD8+CD28-CD27- T Cells Is Associated with Decreased Akt (Ser473) Phosphorylation. J Immunol. 2007; 178:7710–7719. [PubMed: 17548608]
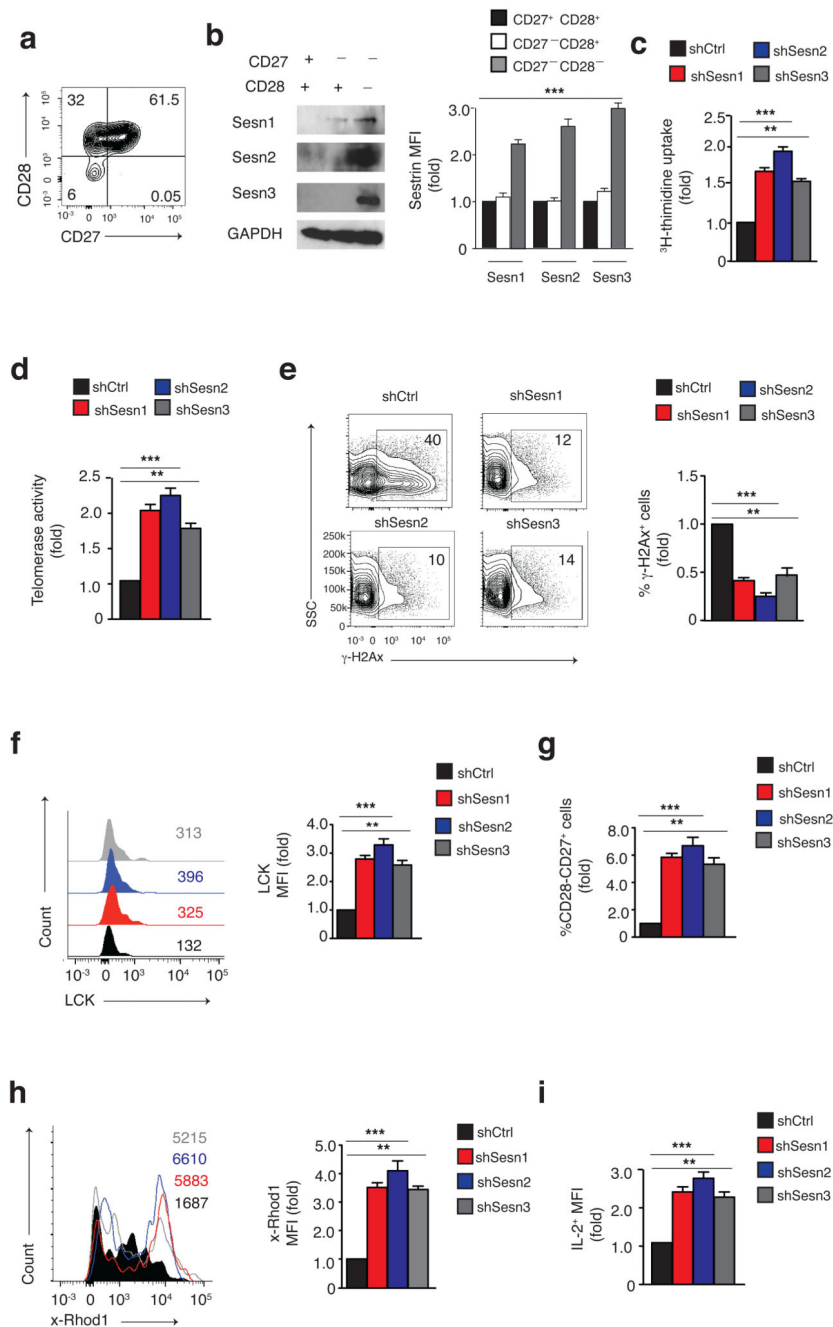
Fig. 1. Sestrins are broad regulators of T cell senescence.
(**a**) Expression of surface CD27 and CD28 in human CD4^{+} T cells by flow-cytometry. (**b**) Immunoblots (left) and flow cytometry data (right) of endogenous sestrin1, sestrin2 and sestrin3 expression in CD4^{+} T cells gated as in (**a**). (**c**) ^{3}H-thymidine uptake and (**d**) telomerase activity in CD4^{+} T$_{sen}$ cells transduced as indicated. (**e**) DNA damage foci assessed by the DNA damage response marker γ-H2Ax in cells as above. Flow cytometry of (**f**) intracellular LCK, (**g**) CD27 and CD28 co-stimulatory receptors, (**h**) calcium abundance and (**i**) IL2 synthesis in CD4^{+} T$_{sen}$ cells transduced as indicated. Results presented relative

to those of cells transduced with shCtrl, set as 1. Data are representative of four experiments (**a, b** (**left**)) or pooled from four experiments with four individual donors (**b** (**right**)) or three donors (**c**, **d**, **e**, **f**, **g**, **h**, **i**). **p<0.01* and ***p< 0.001* calculated using ANOVA for repeated measures with Bonferroni post-test correction. Error bars indicate s.e.m.
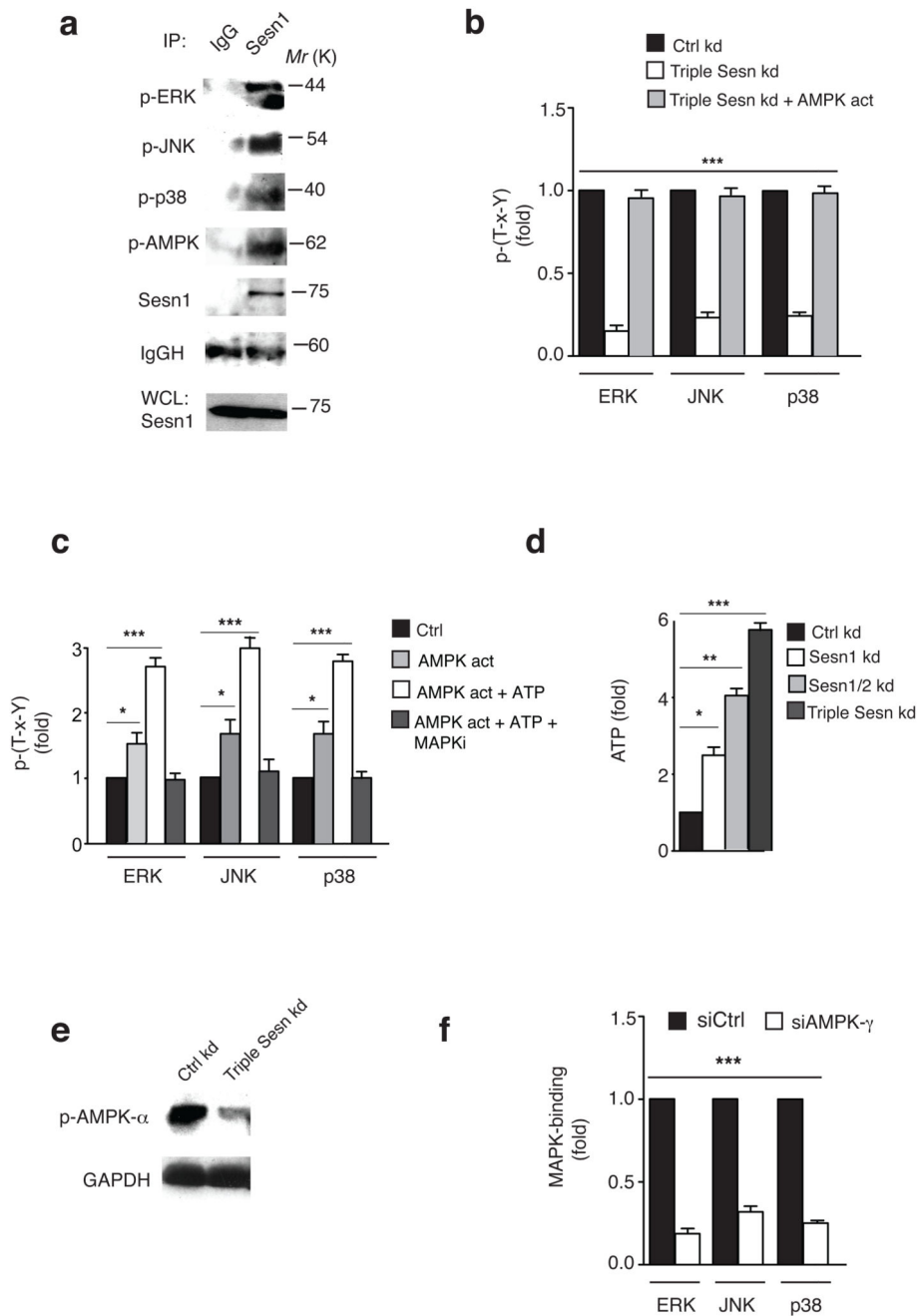
Fig. 2. Sestrins bind to and activate Erk, Jnk and p38 in T$_{sen}$.
(**a**) Immunoblot analysis of lysates from CD4$^+$ T$_{sen}$ precipitated with IgG control or sestrin1 antibodies, and stained for the indicated proteins. Right margin, molecular weights. (**b**) MAPK phosphorylation of AMPK immunoprecipitates from CD4$^+$ T$_{sen}$ transduced as indicated then treated with the AMPK agonist A-769662 (150 μM, 60') 96h later. Results assessed by *in vitro* kinase assay based on an enzyme-linked immunosorbent assay (absorbance at 450 nm) and presented relative to that of cells transduced with shCtrl, set as 1. (**c**) MAPK auto-phosphorylation in sestrin1 complexes from CD4$^+$ T$_{sen}$ incubated for 30'

with the AMPK agonist A-769662 (150 μM, 30'), the Erk inhibitor FR18024 (20 μM), the Jnk inhibitor SP-600125 (10 μM) or the p38 inhibitor SB-203580 (10 μM), in the presence or absence of ATP (200 μM). MAPK activity was determined and presented as in (**b**). (**d**) ELISA-based ATP abundance in AMPK-γ immunoprecipitates from CD4$^+$ T$_{sen}$ whereby one or more sestrins were silenced by shRNA. Results presented relative to that of cells transduced with shCtrl, set as 1. (**e**) AMPK phosphorylation of cells as in (**d**); GAPDH, loading control. (**f**) Elisa-based MAPK-binding assays in sestrin1 immunoprecipitates from cells as in (**a**) transfected with either Ctrl or siAMPK-γ for 36h, and presented relative to those of cells transfected with siCtrl, set as 1. Data are representative of two (**a**) or three (**e**) experiments or pooled from three independent experiments with three individual donors (**b**, **c, d, f**). *$p<0.05$ **$p<0.01$ and ***$p< 0.001$, ANOVA for repeated measures with Bonferroni post-test correction. Error bars indicate s.e.m. throughout.
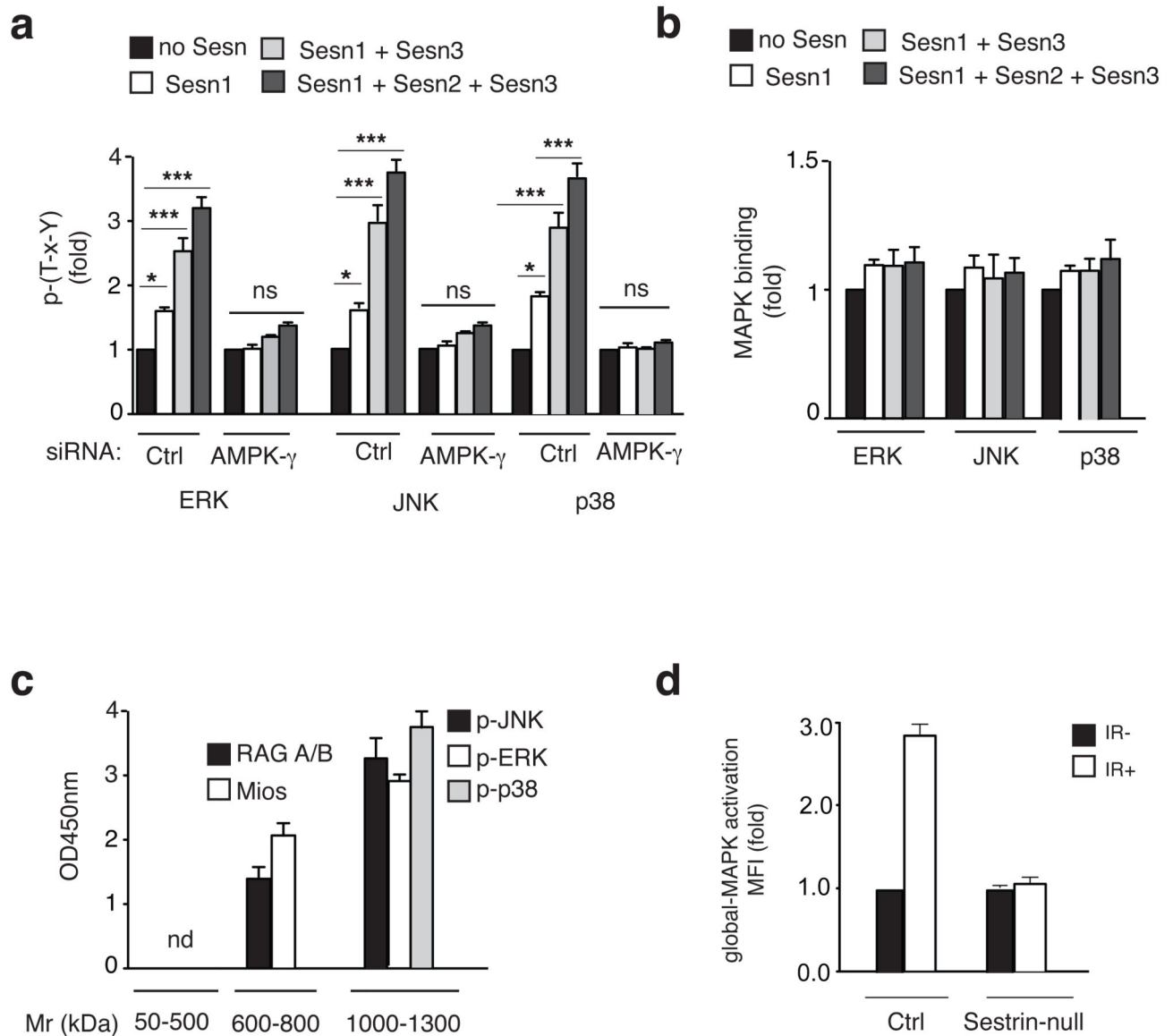
Fig. 3. Reconstitution of the sMAC in T_{erl}.
(**a**) ELISA-based MAPK phosphorylation in AMPK immunoprecipitates from CD4+ T_{erl} cells transfected as indicated, lysed 36h later, and incubated with either GFP ('no Sesn') or recombinant human sestrins (1 μg/mL, each) for 1h. Sestrin-dependent MAPK activation presented relative to that of GFP-treated extracts ('no Sesn'), set as 1. (**b**) ELISA-based MAPK binding in lysates from CD4+ T_{erl} cells, incubated with recombinant sestrins for 1h followed by immunoprecipitation with AMPK antibodies. MAPK recruitment to AMPK presented relative to that of GFP-treated extracts ('no Sesn'). (**c**) Gel-filtration chromatography coupled to ELISA-binding assays of sestrin2 complexes from CD4+ T_{erl} cells after incubation with recombinant sestrins. **d**) Irradiation-triggered Erk, Jnk and p38 phosphorylation in CD4+ T_{erl} transduced as indicated, then analyzed by phospho-flow 8h after radiation. Data are pooled from three (**a**) or two (**b,c,d**) independent experiments.

p<0.05 *p<0.01* and ****p< 0.001,* ANOVA for repeated measures with Bonferroni post-test correction. Error bars indicate s.e.m. throughout.
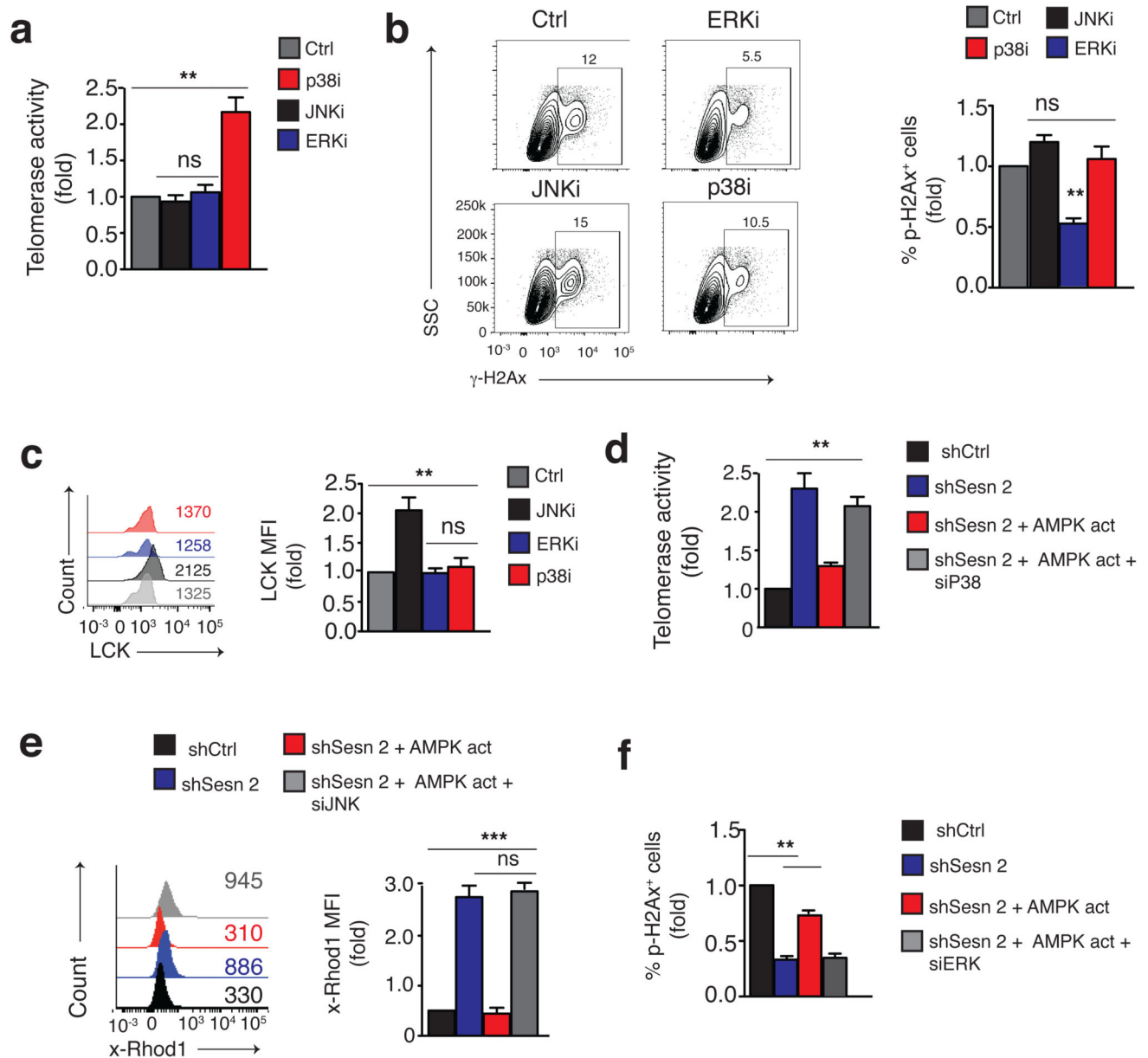
Fig. 4. Individual MAPKs control different aspects of T cell senescence

Measurement of (**a**) telomerase activity, (**b**) endogenous DDR foci and (**c**) expression of the TCR signalosome component LCK in CD4$^+$ T$_{sen}$ cells treated with the Erk inhibitor FR18024 (20 μM), the Jnk inhibitor SP-600125 (10 μM) or the p38 inhibitor SB-203580 (10 μM) for 36 hours, then analysed for functional readouts. A DMSO solution was used as control. (**e-g**) Effect of the indicated siRNAs on (**d**) telomerase activity, (**e**) calcium flux and (**f**) DDR foci in sestrin2-silenced CD4$^+$ T$_{sen}$ treated with the AMPK agonist A-769662 (150 μM, 48 hours). Data pooled from four independent experiments with four individual donors (**a**, **b**, **c**) or three independent experiments (**d**, **e**, **f**), and presented relative to those of cells transfected or transduced with siCtrl or shCtrl, set as 1. ***p<0.01* and ****p< 0.001,* ANOVA

for repeated measures with Bonferroni post-test correction. Error bars indicate s.e.m. throughout.
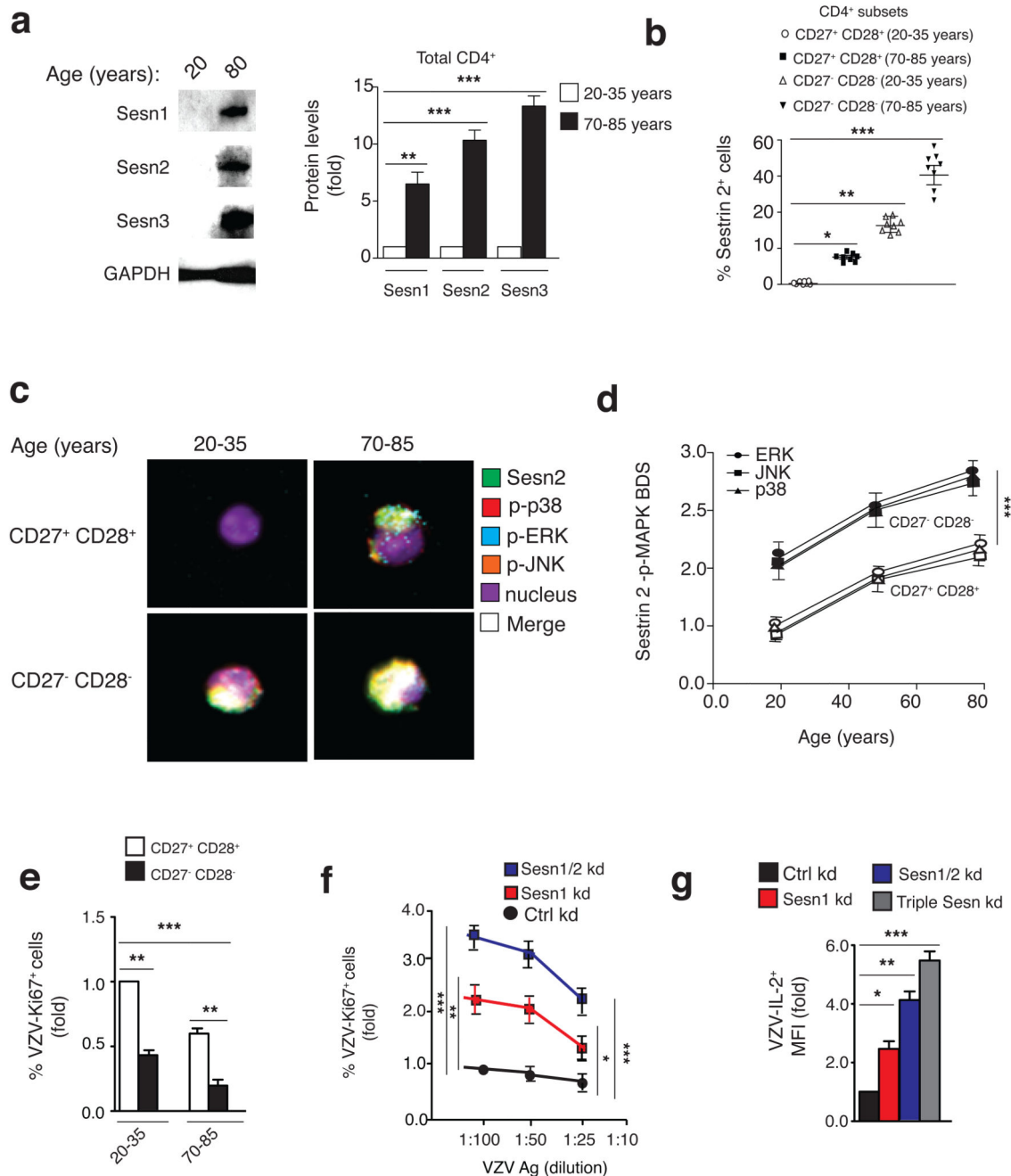
Fig. 5. Enhanced sMAC formation with age.
(**a**) Immunoblots (left) and data (right) of endogenous sestrin proteins in lysates from young (20-35 years) *versus* old (70-85 years) primary human CD4$^+$ T cells. Age-dependent expression of sestrins was normalized to endogenous GAPDH and presented relative to that of young donors, set as 1. (**b**) Flow-cytometry assessing sestrin2$^+$ cells among CD4$^+$ T$_{erl}$ and CD4$^+$ T$_{sen}$ subsets from 8 young and 8 old individuals. (**c**) Age-dependent sMAC formation by Image Stream in cells as in (**b**); representative of several images from 4 different individuals per each age-group. (**d**) Sestrin2$^+$-p-MAPKs$^+$ co-localization scores

(BDS) of cells as in (**c**) ($n = 4$). (**e**) VZV-specific proliferation in CD4$^+$ T$_{erl}$ and CD4$^+$ T$_{sen}$ cells from 3 young and 3 old donors. Pooled data ($n = 3$) presented relative to those of CD4$^+$ T$_{erl}$ from young donors, set as 1. (**f**) Restored VZV-specific sensitivity (proliferation) in CD4$^+$ T$_{sen}$ from old humans where one or two Sestrins were silenced by shRNA ($n = 3$), presented relative to that of cells transduced with shCtrl and stimulated with the lowest VZV antigen dilution (1:100), set as 1. (**g**) Restored IL2 synthesis in sestrin-silenced CD4$^+$ T$_{sen}$ reactivated with autologous APCs loaded with a VZV antigen dilution of 1:100 and presented as in (**f**) ($n = 3$). Data are pooled from three experiments with three separate donors (**a, e, f, g**) or four experiments with eight (**b**) or four (**c, d**) donors. *$p<0.05$ **$p<0.01$ and ***$p< 0.001$, ANOVA for repeated measures with Bonferroni post-test correction. Error bars indicate s.e.m. throughout.
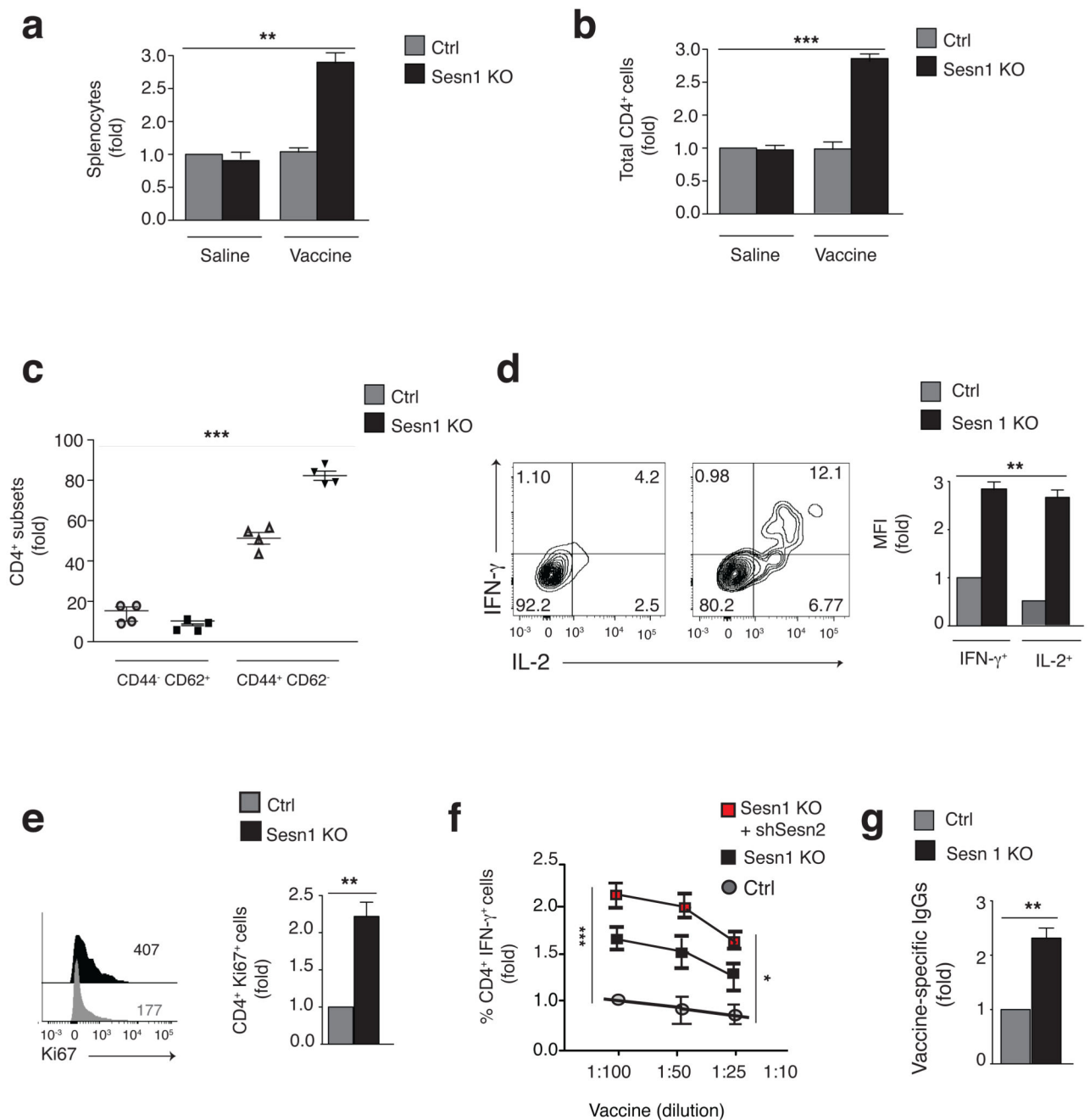
Fig. 6. Sestrin deficiency enhances responsiveness to vaccination in old mice.
(**a**) Splenocyte count of 20-month $Sesn1^{+/-}$ and $Sesn1^{-/-}$ mice vaccinated with FLUAD (1:20 of human dose) or vehicle saline solution, then culled 5 days later. (**b**) Absolute CD4$^+$ T cell count in mice as in (**a**). (**c**) Frequencies of naïve CD62L$^+$ CD44$^-$ and effector CD62L$^-$ CD44$^+$ CD4$^+$ T cells in $Sesn1^{+/-}$ and $Sesn1^{-/-}$ mice vaccinated with FLUAD. (**d**) Counter-plots (left) and MFI data (right) showing IFN-γ and IL-2 production among CD4$^+$ T cells from $Sesn1^{+/-}$ and $Sesn1^{-/-}$ mice after FLUAD-vaccination. Pooled results ($n = 4$) presented relative to those of vaccinated $Sesn1^{+/-}$ mice, set as 1. (**e**) Proliferation among CD4$^+$ T cells

from mice as in (**d**), representative overlay and pooled data ($n = 4$). (**f**) IFN-γ production in *Sesn1*$^{+/-}$ and *Sesn1*$^{-/-}$ CD4$^+$ T cells after FLUAD-vaccination, transfected as indicated then re-stimulated for 18h with *Sesn1*$^{+/-}$ APCs pre-loaded with FLUAD. Results presented relative to that of vaccinated *Sesn1*$^{+/-}$ mice, set as 1. (**g**) One-week vaccine-specific IgG titers in serum of vaccinated *Sesn1*$^{+/-}$ or *Sesn1*$^{-/-}$ mice. ELISA-based binding assays presented relative to those of vaccinated *Sesn1*$^{+/-}$ mice, set as 1. Data are from two experiments with six (**a, b**) or four (**c**, **d, e, g**) individual aged-matched mice per group or three independent experiments with three individual mice per group (**f**). *$p<0.05$ **$p<0.01$ and ***$p< 0.001$,* ANOVA for repeated measures with Bonferroni post-test correction (**a, b, c, f**) or paired Student's *t*-test (**d, e, g**). Error bars indicate s.e.m. throughout.
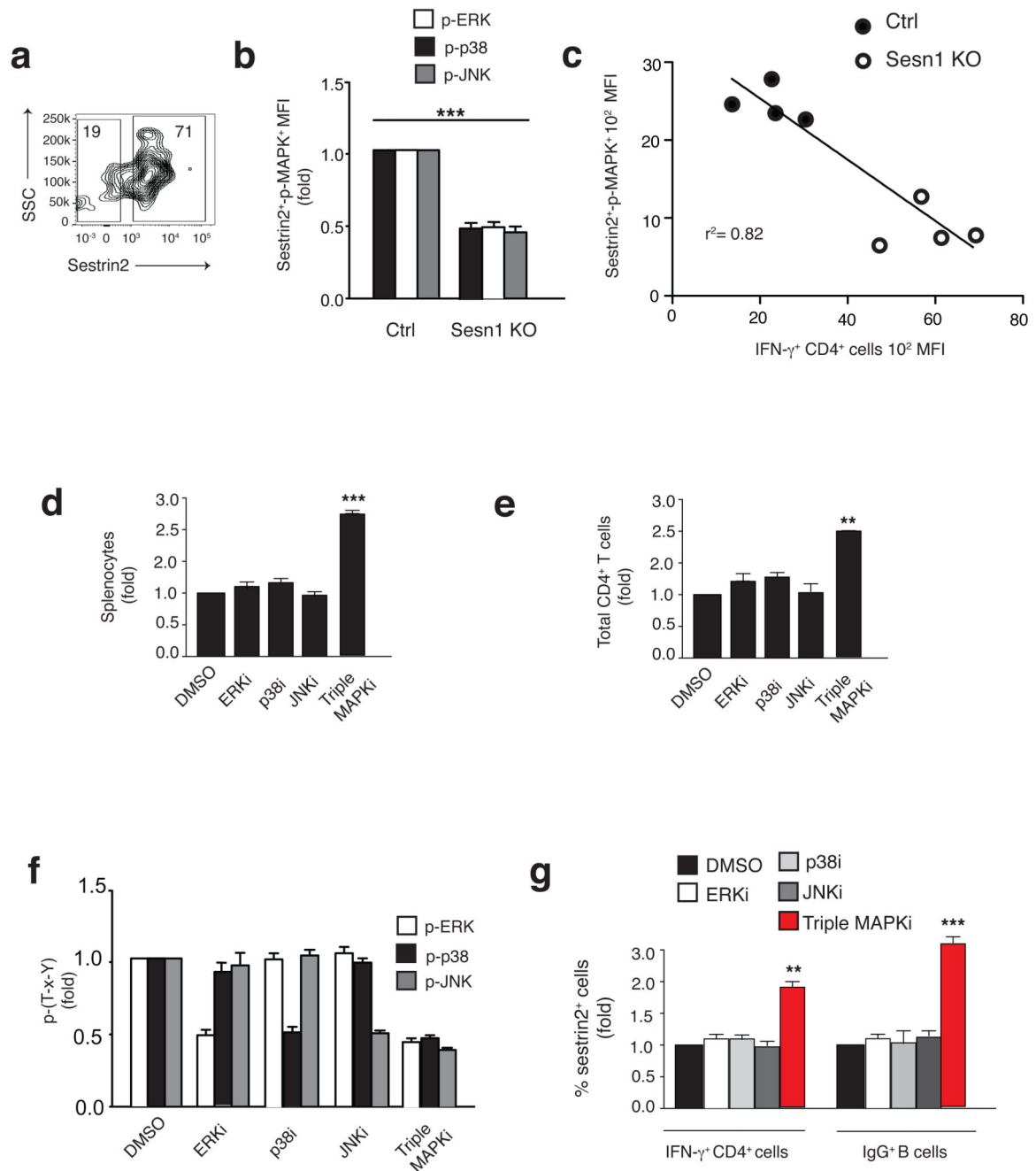
Fig. 7. Simultaneous MAPKi phenocopies Sestrin-deficiency *in vivo*
(**a**) Phospho-flow analysis of sestrin2 expression in CD4^{+} T cells from 16-month old mice.
(**b**) Erk, Jnk and p38 phosphorylation in CD4^{+} T cells from control *Sesn1*^{+/-} and *Sesn1*^{-/-}
mice (20 months) vaccinated as in Figure 6. Data (*n = 4*) presented relative to those of
control *Sesn1*^{+/-} mice, set as 1. (**c**) Correlation between reduced sestrin2^{+}-p-Erk^{+}/p-Jnk^{+}/p-
p38^{+} signaling and enhanced IFN-γ^{+} production in CD4^{+} T cells from *Sesn1*^{-/-} versus
Sesn1^{+/-} mice after FLUAD vaccination (*n = 4*; *r*[2] *= 0.82*). (**d**) Splenocyte and (**e**) CD4^{+} T
cell counts from 16-old mice injected with Erk (25 mg/kg), Jnk (16 mg/kg) and p38 (10

mg/kg) inhibitors either individually or together (triple MAPKi), vaccinated with FLUAD, and daily kept on MAPKi for five days. Results relative to those of DMSO-treated mice, set as 1. (**f**) MAPK-self phosphorylation in CD4$^+$ T cells from mice as in (**d-e**) assessed by *in vitro* kinase assays, and presented relative to those of DMSO treated mice, set as 1. (**g**) FLUAD-driven IFN-γ production and IgG isotypic-switch among sestrin2$^+$ CD4$^+$ T and CD19$^+$ B cells in mice as in (**d-e**), assessed by flow-cytometry. Pooled data ($n = 4$) presented relative to those of DMSO treated mice, set as 1. Data are pooled from four experiments with four (age-matched) mice per group (**a**, **b, c, d, e, g**) or two experiments (**f**). **$p<0.01$ and ***$p< 0.001,$ ANOVA for repeated measures with Bonferroni post-test correction. Error bars indicate s.e.m. throughout. r^2, Pearson-correlation test.
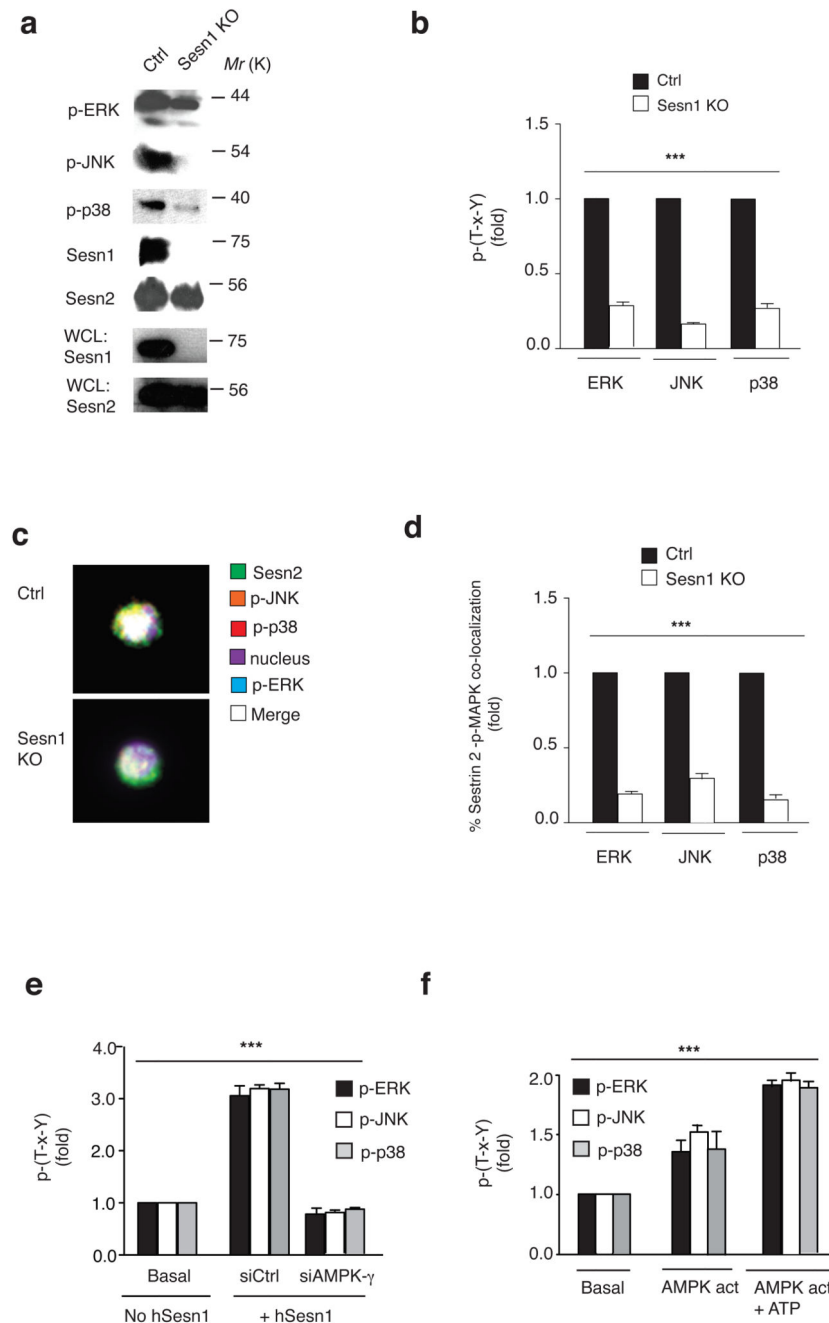
Fig. 8. The sMAC is formed in mouse T cells.
(**a**) Immunoblot analysis and (**b**) pooled data (*n = 4*) of Erk, Jnk, and p38 phosphorylation in lysates from CD4^{+} T cells from 20-month old vaccinated *Sesn1^{+/-}* and *Sesn1^{-/-}* mice following immunoprecipitation with sestrin2 antibodies. Results in (**b**) presented relative to those of *Sesn1^{+/-}* mice, set as 1. Sestrin2 expression in whole cell lysates (WCL), loading control. Sestrin1 expression is also shown. (**c**) Image-Stream analysis and (**d**) % co-localization scores of sestrin2^{+}-pMAPKs^{+} in CD4^{+} T cells from *Sesn1^{-/-}* and *Sesn1^{-/+}* mice, five days post-vaccination with FLUAD, presented as in (**b**). *In vitro* MAPK assays of

sestrin2 immunoprecipitates from mouse *Sesn1*$^{-/-}$ CD4$^+$ T cells incubated for 60' with or without (**e**) recombinant human sestrin1 or (**f**) the AMPK agonist A-769662, in the presence or absence of ATP. Results presented relative to that of non-reconstituted *Sesn1*$^{-/-}$ cells ('basal'), set as 1. In (**e**) cells were transfected with the indicated siRNAs 48h before lysis. Data are representative of four experiments (**a, c**) or pooled from four experiments with four (age-matched) individual mice (**b**, **d**, **e**, **f**). ***p<0.01** and ****p< 0.001,* ANOVA for repeated measures with Bonferroni post-test correction. Error bars indicate s.e.m. throughout.